Protein kinase D2 induces invasion of pancreatic cancer cells by regulating matrix metalloproteinases

Christoph Wille[a,*], Conny Köhler[b,*], Milena Armacki[a], Arsia Jamali[b], Ulrike Gössele[a], Klaus Pfizenmaier[c], Thomas Seufferlein[a,†], and Tim Eiseler[a,†]

[a]Department of Internal Medicine I, Ulm University, D-89081 Ulm, Germany; [b]Department of Internal Medicine I, Martin-Luther University Halle-Wittenberg, D-06120 Halle (Saale), Germany; [c]Institute for Cell Biology and Immunology, University of Stuttgart, D-70569 Stuttgart, Germany

ABSTRACT **Pancreatic cancer cell invasion, metastasis, and angiogenesis are major challenges for the development of novel therapeutic strategies. Protein kinase D (PKD) isoforms are involved in controlling tumor cell motility, angiogenesis, and metastasis. In particular PKD2 expression is up-regulated in pancreatic cancer, whereas PKD1 expression is lowered. We report that both kinases control pancreatic cancer cell invasive properties in an isoform-specific manner. PKD2 enhances invasion in three-dimensional extracellular matrix (3D-ECM) cultures by stimulating expression and secretion of matrix metalloproteinases 7 and 9 (MMP7/9), by which MMP7 is likely to act upstream of MMP9. Knockdown of MMP7/9 blocks PKD2-mediated invasion in 3D-ECM assays and in vivo using tumors growing on chorioallantois membranes. Furthermore, MMP9 enhances PKD2-mediated tumor angiogenesis by releasing extracellular matrix–bound vascular endothelial growth factor A, increasing its bioavailability and angiogenesis. Of interest, specific knockdown of PKD1 in PKD2-expressing pancreatic cancer cells further enhanced the invasive properties in 3D-ECM systems by generating a high-motility phenotype. Loss of PKD1 thus may be beneficial for tumor cells to enhance their matrix-invading abilities. In conclusion, we define for the first time PKD1 and 2 isoform–selective effects on pancreatic cancer cell invasion and angiogenesis, in vitro and in vivo, addressing PKD isoform specificity as a major factor for future therapeutic strategies.**

Monitoring Editor
Josephine C. Adams
University of Bristol

Received: Jun 20, 2013
Revised: Nov 25, 2013
Accepted: Dec 2, 2013

INTRODUCTION

A hallmark of pancreatic ductal adenocarcinomas (PDACs) is perineural and retroperitoneal invasion of tumor cells, impairing treatment of primary tumors by surgical resection (del Castillo and Warshaw, 1993; Crawford *et al.*, 2002; Egeblad and Werb, 2002; Porzner and Seufferlein, 2011). Strategies to control invasive properties of a tumor are vital to improve treatment options. Protein kinase D isoforms PKD1 (PKCμ), 2, and 3 are regulators of different pathways controlling transcriptional regulation of cancer-relevant target genes, actin-regulatory proteins, angiogenesis, and tumor cell motility (Rykx *et al.*, 2003; Eiseler *et al.*, 2009b, 2010a; Azoitei *et al.*, 2010; Armacki *et al.*, 2013). Degradation of the extracellular matrix (ECM) and breakdown of basal membranes by matrix metalloproteinases (MMPs) constitute key steps in cancer cell invasion and eventually metastasis (Egeblad and Werb, 2002). PKDs have been implicated in the regulation of MMPs in prostate cancer cells (Biswas *et al.*, 2010; LaValle *et al.*, 2012), stromal myofibroblasts (Yoo *et al.*, 2011), and breast cancer cells (Eiseler *et al.*, 2009a). Studies in prostate cancer cells mainly focused on PKD1- or 3-dependent regulation of MMP9/2 modulating proliferation (Biswas *et al.*, 2010; LaValle *et al.*, 2012). We previously showed that PKD1 expression is

This article was published online ahead of print in MBoC in Press (http://www.molbiolcell.org/cgi/doi/10.1091/mbc.E13-06-0334) December 11, 2013.

*These authors contributed equally.

†These should be considered co–last authors.

T.E. and T.S. conceived the study. C.W., C.K., A.J., U.G., M.A., and T.E. performed experiments and evaluated data. T.E. and T.S. wrote the manuscript.

The authors declare no conflict of interest.

Address correspondence to: Tim Eiseler (tim.eiseler@uniklinik-ulm.de).

Abbreviations used: FRAP, fluorescence recovery after photobleaching; FRET, Foerster energy transfer; GFP, green fluorescence protein; ROI, region of interest.

down-regulated in breast cancer cells (Eiseler *et al.*, 2009a) but inhibits expression of distinct MMPs (Eiseler *et al.*, 2009a). In addition, PKD1 impairs the motility of tumor cells, including breast and pancreatic cancer cells (Eiseler *et al.*, 2007, 2009b, 2010a). PKD2, on the other hand, is up-regulated in pancreatic tumors (Seufferlein, 2002; Azoitei *et al.*, 2010; Porzner and Seufferlein, 2011). We showed that this kinase isoform stimulates tumor angiogenesis by transcriptional up-regulation and secretion of vascular endothelial growth factor A (VEGF-A; Azoitei *et al.*, 2010; Armacki *et al.*, 2013). Here we identify PKD2 as key upstream regulator of MMP7 and 9. MMPs are expressed as inactive proenzymes. MMPs are activated by a combination of cleavage in the prodomain and cleavage between the prodomain and the catalytic domain. All MMPs are synthesized with a signal peptide, which is subsequently cleaved during transport through the secretory pathway (Page-McCaw *et al.*, 2007). Both MMP7 (matrilysin) and MMP9 are members of the zinc-dependent extracellular proteases (Werb, 1997; Egeblad and Werb, 2002; Kessenbrock *et al.*, 2010). Many MMP7 substrates are components of the extracellular matrix (Crawford *et al.*, 2002). MMP7 is expressed in 98% of well-differentiated PDACs and 100% of metaplastic duct epithelium. MMP7 is also associated with the formation of preneoplastic pancreatic lesions in vivo (Crawford *et al.*, 2002; Egeblad and Werb, 2002). MMP9 is a member of the gelatinase MMP subfamily, with three fibronectin-domain inserts in its catalytic domain (Page-McCaw *et al.*, 2007). MMP9-null mice display defects in postembryonic neovasculature, indicating vital functions during physiological and tumor angiogenesis (Bergers *et al.*, 2000; Tsuzuki *et al.*, 2001; Page-McCaw *et al.*, 2007; Kessenbrock *et al.*, 2010). Of interest, this function has been associated with processing of VEGF-A, which is stored in the extracellular matrix after secretion (Bergers *et al.*, 2000; Korc, 2003). In this study we present a novel isoform-specific regulatory function for PKD2 upstream of MMP 7 and 9 in pancreatic cancer cells, promoting invasion and angiogenesis in vitro and in vivo. We further demonstrate that in marked contrast PKD1 prevents invasion of pancreatic cancer cells. Thus PKD2 is a novel target to prevent tumor cell invasion and angiogenesis.

RESULTS

Because PKD2 is highly expressed in pancreatic cancer, a highly invasive tumor, we initiated this study to investigate a potential PKD2-dependent regulation of MMPs and tumor invasion (Beil *et al.*, 2002; Seufferlein, 2002; Porzner and Seufferlein, 2011).

Expression of PKD isoforms in PDAC and pancreatic cancer cell lines

We performed an initial analysis of microarray data using R2: microarray analysis and visualization platform (http://r2.amc.nl) to confirm the expression of PKD2 mRNA in pancreatic tumors versus normal tissues and in various pancreatic cancer cell lines (Figure 1, A and B). PKD2 mRNA was significantly up-regulated in PDACs of the Wang data set (Pei *et al.*, 2009). PKD2 was also present at elevated levels in a panel of pancreatic cell lines compared with PKD1 mRNA (Maupin *et al.*, 2010). We also investigated protein expression of all PKD isoforms in a panel of pancreatic cancer cell lines (Supplemental Figure S1A). PKD1 and 2 were present at higher levels in Panc89 and 1 cells. PKD3 was expressed at equal levels in all cell lines tested. Thus we used Panc89 cells to generate stable cell lines for subsequent studies expressing green fluorescent protein (GFP)–Vector, PKD1-GFP, and PKD2-GFP (Eiseler *et al.*, 2012). Expression levels of transgenes in the respective stable cell lines were subsequently verified by Western blot and flow cytometry (Supplemental Figure S1, B and D). PKD1 and 2 specificity controls for antibodies used in this study are shown in Supplemental Figure S1, B and C.

Differential control of pancreatic tumor cell invasion by PKD1 and 2

Because perineural and retroperitoneal invasion is a hallmark of pancreatic cancer (del Castillo and Warshaw, 1993; Guha *et al.*, 2010; Porzner and Seufferlein, 2011), we investigated whether PKD1 and 2 could regulate the invasive properties of tumor cells in a three-dimensional (3D)-ECM culture system. Using Panc89 cells stably expressing PKD1- or PKD2-GFP, we showed that PKD2 significantly enhanced outgrowth of tumor cells from primary clusters into the surrounding matrix by ~40% compared with vector controls, whereas PKD1 significantly inhibited invasion by ~13% after 16 d. The latter observation was in line with our data for breast cancer cells (Eiseler *et al.*, 2009a; Figure 2, A and B). To corroborate this novel PKD2 phenotype, we performed an inverse experiment using two different short hairpin RNAs (shRNAs) for PKD2 in GFP-Vector control cells (Figure 2, C–E). Knockdown of PKD2 significantly impaired invasion of tumor cells into the surrounding 3D-matrix by 48.3 and 34.4%, respectively. As shown previously (Eiseler *et al.*, 2009a), knockdown of PKD1 in tumor cells significantly enhances tumor cell invasion (Supplemental Figure S1E) but inhibits proliferation of pancreatic cancer cells (Eiseler *et al.*, 2012).

Invasion of tumor cells into the ECM requires the degradation of matrix proteins by MMPs. We therefore investigated whether PKD2-mediated enhanced invasion could be attributed to MMP regulation.

PKD2 enhances expression of distinct matrix metalloproteinases

We performed 3D-ECM assays in the presence of 1 µM Marimastat (Rasmussen and McCann, 1997; Figure 3, A and B), which inhibits MMP1, 2, 7, 9, and 14 at nanomolar concentrations. Expression of PKD2-GFP strongly enhanced pancreatic cancer cell invasion into the matrix as compared with vector controls. Marimastat abolished PKD2-driven invasion in the 3D-ECM culture, indicating that Marimastat-sensitive MMPs are responsible for the PKD2 invasion phenotype. To identify the respective MMPs regulated by PKD2, we performed a quantitative PCR (qPCR) screen for mRNA levels of these MMPs in Panc89 cells stably expressing GFP-Vector, PKD1-GFP, or PKD2-GFP (unpublished data). These experiments revealed the matripase, MMP7, and the gelatinase, MMP9, as Marimastat-sensitive MMPs, which were significantly up-regulated by ~11-fold in PKD2-expressing cells. PKD1 only had a minor effect on MMP9 and no effect on MMP7 expression (Figure 3C). Transcriptional regulation was also verified at the protein level by Western blot (Supplemental Figure S2A). Activity of MMPs was examined using gelatin zymography from concentrated cell culture supernatants of Panc89 GFP-Vector and PKD2-GFP cells (Supplemental Figure S2B).

PKD2 controls secretion of MMP7 and 9 in an isoform-specific manner

In addition to transcriptional regulation, PKDs control the release of secretory cargo vesicles at the *trans*-Golgi network (TGN; Yeaman *et al.*, 2004; Pusapati *et al.*, 2010). PKD2 might thus modulate MMP7 and 9 at further levels. We first examined MMP7 and 9 localization at the TGN in Panc1 cells. Both MMPs colocalized with the TGN-resident proteins TGN46 and golgin97 (Pusapati *et al.*, 2010; Supplemental Figure S3A). To determine whether MMP7 and 9 were secreted from cells in a PKD2 isoform–specific manner, we performed secretion assays using ectopically expressed MMP7–yellow fluorescent protein

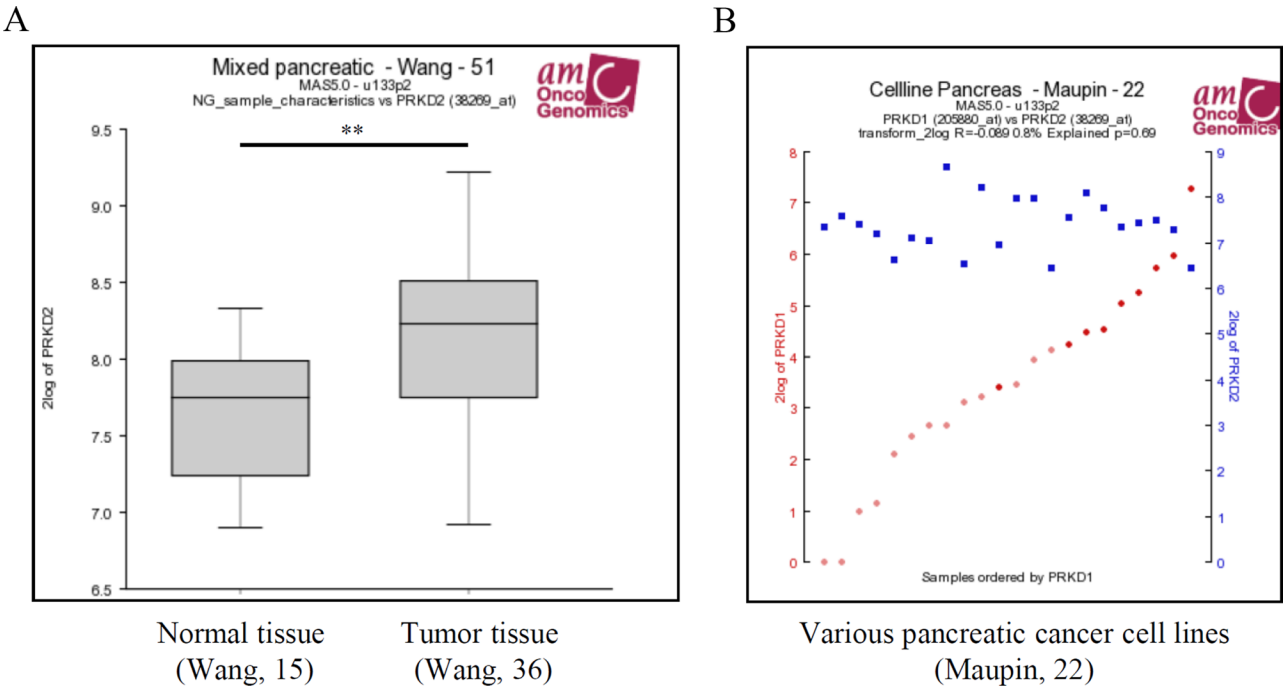

FIGURE 1: Meta-analysis of PKD2 and PKD1 mRNA expression data using R2: microarray analysis and visualization platform (http://r2.amc.nl). (A) PKD2 mRNA is significantly higher when expressed in tumor samples vs. control tissue. Meta-analysis of a tumor sample data set provided by the group of L. Wang (Pei *et al.*, 2009). Statistical analysis was performed using a one-way analysis of variance (ANOVA) test. (B) PKD2 mRNA levels are higher than PKD1 mRNA in various pancreatic cancer cell lines of the Maupin data set (Maupin *et al.*, 2010). mRNA expression of PKD2 (blue) blotted vs. PKD1 (red).

(YFP) or YFP-MMP9 in HEK293T cells depleted of PKD1 or PKD2, respectively. Of interest, only knockdown of PKD2 led to a marked inhibition of MMP9 and 7 secretion. Knockdown of PKD1 had hardly any effect (Supplemental Figure S3B). We also determined MMP9 cargo release from the TGN using a modified fluorescence recovery after photobleaching (FRAP) approach in HeLa cells expressing MMP9-GFP together with constitutively active PKD1SSEE or PKD2SSEE. In these cells MMP9-GFP colocalized with TGN46 and golgin97 (Supplemental Figure S3C). Provided that influx of cargo into the TGN compartment is equal, recovery of fluorescence at the TGN is modulated by release of secretory vesicles during constitutive secretion. In line with secretion assays in HEK293T cells (Supplemental Figure S3B), FRAP data revealed at the single-cell level that only constitutively active PKD2SSEE, and not PKD1SSEE, is capable of significantly enhancing release of MMP9-GFP–containing vesicles from the TGN (Supplemental Figure S3, D and E).

To validate these findings in pancreatic cancer cells, we examined secretion of endogenous MMP7 and 9 from Panc89 and 1 cells after knockdown of PKD1 or 2, respectively. In Panc89 cells, knockdown of PKD2 significantly impaired secretion of endogenous MMP9 and 7 by 41.3 and 49.5%, respectively (Figure 4A). Knockdown of PKD1 had a minor nonsignificant effect on endogenous MMP9 and no effect on MMP7 secretion (Figure 4A). The latter is in line with the literature (Merikallio *et al.*, 2012) and our qPCR experiments demonstrating a minor transcriptional up-regulation of MMP9 by PKD1 (Figure 3C), which could be mediated via Snail1 (Eiseler *et al.*, 2012). In Panc1 cells, knockdown of PKD2 also significantly impaired endogenous secretion of MMP9 by 58.1% and MMP7 by 65.1%. Knockdown of PKD1 impaired MMP9 secretion by only 29.3% and had very little effect on MMP7 secretion (15.7%; Figure 4B). Knockdown controls and secreted MMP7 probed in supernatants are shown in Supplemental Figure S3F. Thus, in contrast to PKD1, PKD2 is the major regulator of MMP7 and 9 secretion in pancreatic cancer cells.

Knockdown of MMP7/9 impairs invasion and angiogenesis of PKD2-expressing pancreatic cancer cells in fibroblast monolayers, 3D-ECM, and chorioallantois membrane assays

To determine whether PKD2-mediated invasion was affected by MMP7/9 secretion from pancreatic cancer cells, we performed fibroblast overlay invasion assays using a combination of MMP-Inhibitor II (1 μM) and MMP9-Inhibitor I (40 nM) to completely inhibit target proteases. At the indicated concentration used, MMP9-Inhibitor I is specific. MMP-Inhibitor II inhibits MMP7, 1, 3, and also 9 at different concentrations. Thus we additionally examined the regulation of MMP1 and 3 in our stable Panc89 cell lines. MMP1 was not regulated compared with GFP-Vector controls by PKD2-GFP, whereas PKD1-GFP induced a slight, nonsignificant transcriptional up-regulation of MMP1 in qPCR (Supplemental Figure S4A). MMP3 was not regulated by PKD1 or 2 (Supplemental Figure S4B). For fibroblast overlay invasion assays we then used transiently transfected Panc1 cells expressing GFP-Vector, constitutively active PKD1SSEE, or PKD2SSEE, incubated with vehicle or the inhibitor cocktail as indicated on the fibroblast monolayers. After 36 h, inactivated, dead fibroblasts were labeled by trypan blue dye, and integrity of monolayers was documented (Figure 5A). Of interest, only Panc1 cells expressing PKD2SSEE-GFP were able to visibly penetrate the fibroblast monolayers in three independent experiments (blue outlines, Figure 5, E′–G′), whereas invasion was blocked by the MMP inhibitor cocktail. In line with the MMP secretion data shown earlier, GFP-Vector– and PKD1SSEE-GFP–expressing cells failed to invade the fibroblast monolayers after 36 h, indicating that the invasive properties

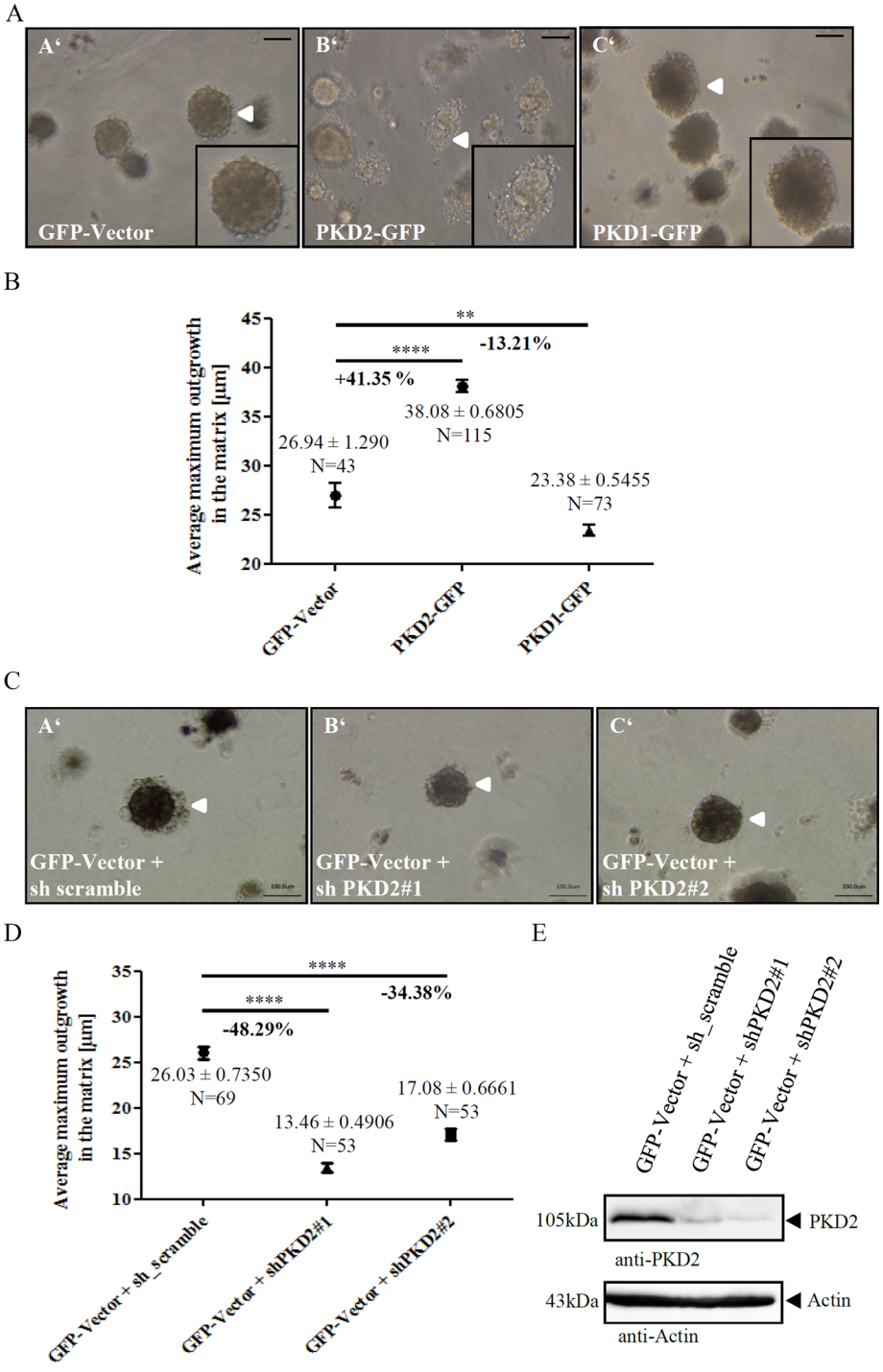

FIGURE 2: Ectopic expression of PKD2 enhances invasion of PDAC cells in the surrounding matrix, whereas expression of PKD1 inhibits invasive outgrowth as compared with vector controls. The 3D-ECM assays of Panc89 cells expressing GFP-Vector, PKD1-GFP, and PKD2-GFP (A′–C′). (A) Assays were documented after 16 d at 10× magnification. (B) Average maximum outgrowth and SEM of three independent experiments. Maximum outgrowth was quantified at five positions around clusters with no more than three measurements within the same outgrowth area using ImageJ. Statistical significance was calculated using two-tailed unpaired Student's *t* test. (C) Knockdown of PKD2 impairs invasive outgrowth in 3D-ECM culture. (A′–C′) GFP-Vector cells expressing sh_scrambled, sh PKD2 #1, and sh PKD2 #2 constructs were seeded in ECM gel. Assays were documented at 12× magnification after 13 d. (D) Average maximum outgrowth and SEM of three independent experiments. Statistical significance was calculated using two-tailed unpaired Student's *t* test. (E) Knockdown of PKD2 was detected in total cell lysates using a PKD2-specific antibody. Actin was used as loading control. Scale bars, 100 µm.

increased only after expression of active PKD2. Experiments with Panc1 cells thus corroborate the data on differential regulation of invasion by PKD1 and 2 (Figure 2).

To examine the specificity of the proposed MMP regulation in more detail, we additionally created stable Panc89 cell lines from GFP-Vector– and PKD2-GFP–expressing cells transduced with shRNAs against MMP7 and 9, as well as nonspecific sh_scramble controls. MMP7 and 9 knockdown, as well as PKD2-GFP transgene expression, was verified (Supplemental Figure S4C), and the cells were subsequently used in 3D basement membrane extract (BME) assays to quantify their respective invasive properties.

The combined stable knockdown of MMP7/9 impaired invasion of GFP-Vector cells into the surrounding matrix by ~26%. PKD2 expression in the nontargeting (sh-scrambled) control cell line strongly enhanced invasion by 145.7%, whereas knockdown of MMP7/9 completely prevented PKD2-mediated outgrowth of Panc89 cells (Figure 5, B and C).

Next we investigated the invasive potential of these stable Panc89 cell lines using an in vivo model system: tumor growth on the chorioallantois membrane (CAM) of fertilized chicken eggs (Azoitei *et al.*, 2010). Panc89 cells expressing GFP-Vector plus sh-scrambled, PKD2-GFP plus sh-scrambled, or PKD2-GFP plus shMMP7/9 were transplanted in Matrigel onto CAM membranes. Hematoxylin and eosin–stained tumor-CAM sections from GFP-Vector plus sh-scrambled cells showed a defined tumor-CAM border, with several cells invading the CAM (Figure 6, A and A′–C′). In comparison, the tumor-CAM border of PKD2-GFP plus sh-scrambled tumors was crossed at several sites. Large multicellular tumor foci were detectable within the mesodermal stroma resembling metastasis-like structures. These data indicate that pancreatic cancer cells expressing PKD2 are indeed different in their invasive capacity, that is, in their ability to successfully form secondary structures during early stages of metastasis (Figure 6, A and D′–G′). The presence of invasive tumor cells in the mesoderm was verified by pan-cytokeratin staining (Armacki *et al.*, 2013; Supplemental Figure S4D). Combined knockdown of MMP7/9 in PKD2-GFP–expressing pancreatic cancer cells reconstituted the clear tumor-CAM border and significantly reduced the invasive capacity (Figure 6, A and H′–J′). To quantify invasiveness, we counted the tumor cell foci in stitched images of the entire tumor-CAM area (Figure 6B).

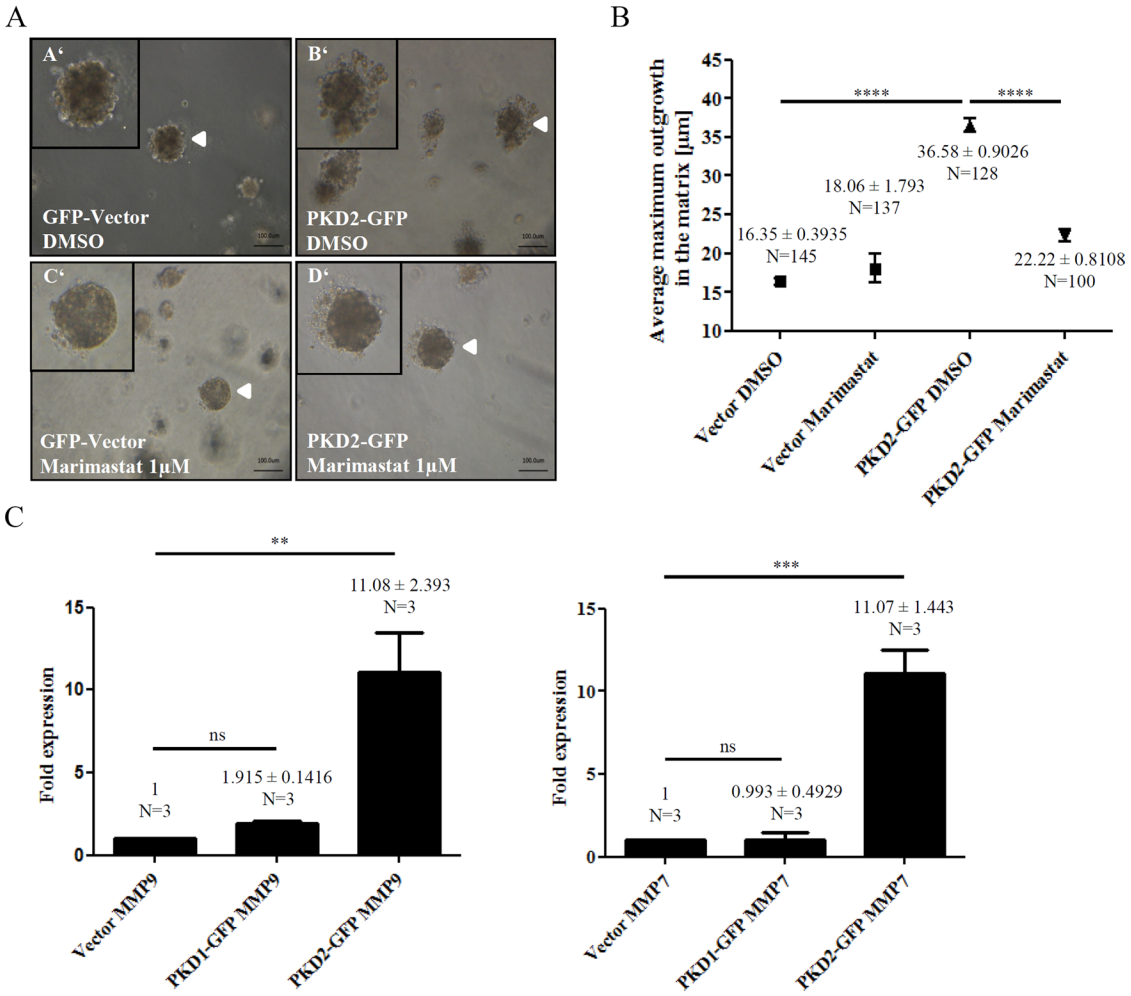

FIGURE 3: Marimastat significantly inhibits invasive outgrowth of PKD2-expressing Panc89 cells in 3D-ECM culture. (A) 3D-ECM assay of GFP-Vector– and PKD2-GFP–expressing Panc89 cells treated with 1 µM Marimastat or vehicle control (dimethyl sulfoxide). After 5 d of growth, a final concentration of 1 µM Marimastat (C′, D′) or vehicle (A′, B′) was added in 500 µl of 3D culture medium. Clusters were documented after 17 d at 10× magnification. Scale bar, 100 µm. (B) Average maximum outgrowth and SEM of three independent experiments. Statistical significance was calculated using two-tailed unpaired Student's *t* test. (C) Transcriptional regulation of MMP7 and 9 expression levels by qPCR in PKD1-GFP– and PKD2-GFP–expressing Panc89 cells in respect to GFP-Vector controls of three independent experiments. Results were calculated according to the ΔΔ*Ct* method normalized to glyceraldehyde 3-phosphate dehydrogenase and vector control cells. Statistical significance was calculated using one-way ANOVA with Dunnett's multiple comparison posttesting.

We previously showed that PKD2 up-regulates VEGF-A expression and secretion in tumor cells (Azoitei *et al.*, 2010). This was also the case in our stable Panc89 cells (Supplemental Figure S4E). To examine angiogenesis, we stained the tumor-CAM sections for the established vessel marker desmin (Azoitei *et al.*, 2010; Armacki *et al.*, 2013). As expected, PKD2-GFP significantly increased desmin-stained areas in CAM tumors. However, the desmin-stained areas were significantly reduced after knockdown of MMP7/9 in the tumors of PKD2-GFP–expressing cells (Figure 6, C and D). These data reveal MMP7/9-dependent regulation of invasion and angiogenesis downstream of PKD2 in pancreatic cancer cells.

MMP9 enhances VEGF-A biorelease by mobilization from ECM

PKD2 up-regulates expression and secretion of VEGF-A (Supplemental Figure S4E; Azoitei *et al.*, 2010). On secretion, VEGF-A binds to the ECM and cellular membranes. Several studies identified MMP9 as a modulator of VEGF-A bioavailability. MMP9 mobilizes VEGF-A from the extracellular matrix and cell surfaces by catalyzing its release from heparan sulfate proteoglycans (Bergers *et al.*, 2000; Bergers and Benjamin, 2003; Masson *et al.*, 2005; Page-McCaw *et al.*, 2007; Kessenbrock *et al.*, 2010). Thus MMP9 could contribute to PKD2-induced angiogenesis by liberating VEGF-A from the ECM. To test this, we performed 3D-ECM assays with PKD2-GFP–expressing tumor clusters exposed to a specific MMP9 inhibitor or solvent for 48 h. Indeed, MMP9 inhibitor–treated, ECM-embedded tumor clusters exhibited a significantly higher intensity value for VEGF-A than the vehicle-treated clusters. These data show that MMP9 secreted from pancreatic cancer cells enhances VEGF-A biorelease from the ECM (Figure 6, E and F, and Supplemental Figure S4F) and add another level of control to PKD2-mediated angiogenesis.

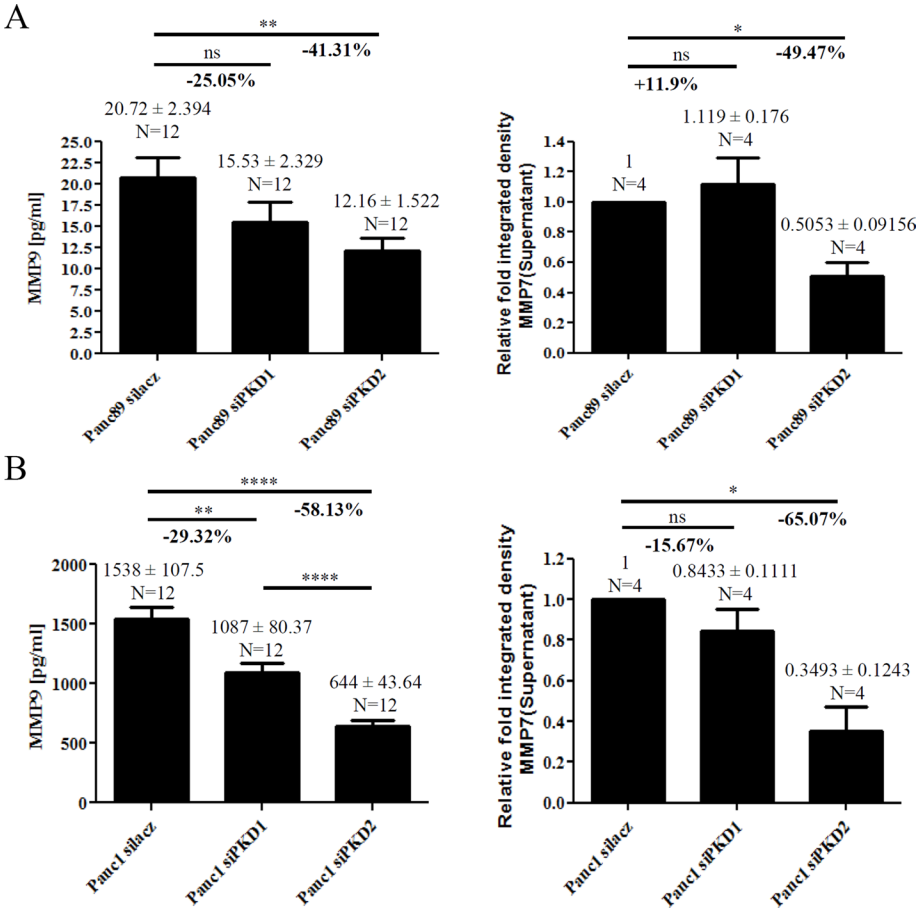

FIGURE 4: Secretion of endogenous MMP7 and 9 is mainly controlled by PKD2. (A) Secretion of endogenous MMP9 after knockdown of PKD1 and 2 in Panc89 cells. After 24 h of secretion in 600 µl of serum-free media, supernatant was harvested and analyzed using a human MMP9 enzyme-linked immunosorbent assay kit. Six independent experiments were performed in duplicate and measured against an MMP9 standard. The graph depicts MMP9 concentrations (pg/ml). MMP7 secretion from Panc89 cells was quantified in Western blots of supernatants by calculating relative integrated densities for MMP7 bands probed with MMP7 antibody. Statistical significance for replica experiments was calculated using two-tailed paired Student's *t* test. (B) Secretion of endogenous MMP7 and 9 after knockdown of PKD1 and 2 in Panc1 cells. After 24 h of secretion, supernatants were harvested and processed as in A.

The effects of PKD1 and 2 on pancreatic cancer cell invasion are isoform specific

Our data so far demonstrate PKD2 isoform–specific control of MMP7/9 expression and secretion that enhances the invasive properties of pancreatic cancer cells and VEGF-A bioavailability in the tumors. Conversely, expression of PKD1 inhibits invasiveness. To emulate a situation frequently occurring in tumors—low expression of PKD1 and high expression of PKD2—we knocked down PKD1 in PKD2-GFP–expressing pancreatic cancer cells and examined invasiveness in 3D-ECM assays (Supplemental Figure S5A). Stable knockdown of PKD1 in PKD2-GFP–expressing cells is verified in Supplemental Figure S5B. Expression of PKD2 plus sh_scramble significantly enhanced invasion compared with the GFP-Vector plus sh_scramble control by ~52.8%. Knockdown of PKD1 in the PKD2-GFP–expressing cell line significantly further enhanced invasion by another 39.5% (Supplemental Figure S5C). These data confirm the proinvasive property of PKD2 and the anti-invasive role of PKD1 in pancreatic tumor cells.

Our data indicate that the PKD1 isoform is hardly contributing to the secretion of MMP7 and 9 from pancreatic cancer cells, which is strongly enhanced by PKD2, thereby modulating invasive properties. Thus loss of PKD1 expression may be a selection advantage for cancer cells by generating a highly motile phenotype, most likely via control of actin regulatory proteins such as Slingshot1L (SSH1L; Eiseler *et al.*, 2007, 2009b, 2010a; Doppler *et al.*, 2013).

SSH1L is a direct PKD substrate. Phosphorylation of Ser-978 by PKD alters F-acting binding and thereby the activity state of the SSH1L phosphatase, which dephosphorylates cofilin and is critically involved in the control of cell motility (Eiseler *et al.*, 2009b). Both PKD1 and PKD2 have been implicated in the regulation of SSH1L by direct phosphorylation (Peterburs *et al.*, 2009). Thus, how is PKD1 able to inhibit cell motility and invasion by phosphorylation of SSH1L at Ser-978 in an isoform-specific manner?

To investigate this question in more detail, we performed fluorescence resonance energy transfer (FRET) interaction studies of PKD1 and 2 with SSH1L in Panc1 pancreatic cancer and in HeLa cells (Supplemental Figure S5, D–I). Performing a sub–region of interest (ROI) analysis of acceptor-photobleach FRET data, we found that in both cell lines PKD1-GFP as compared with PKD2-GFP preferentially interacted with endogenous SSH1L at the cell periphery and in peripheral membrane protrusions. In Panc1 cells, interaction of PKD2-GFP with SSH1L was significantly impaired by 77.3% with respect to the PKD1-GFP–SSH1L interaction (Supplemental Figure S5D), whereas in HeLa cells the interaction of PKD2-GFP with SSH1L was significantly impaired by 64.34% with respect to PKD1 (Supplemental Figure 5F). In a reverse approach we also evaluated the interaction of endogenous PKD1 and 2 with SSH1L-myc in Panc1 cells (Supplemental Figure S5E). Again, interaction of endogenous PKD2 with SSH1L-myc in the cell periphery was significantly impaired by 83.4% compared with endogenous PKD1, strongly supporting an isoform-specific, migratory-relevant regulation of SSH1L by PKD1 at dynamic peripheral cellular structures, such as membrane ruffles and cellular protrusions (Supplemental Figure S5, G–I). However, in the cytoplasm and in the perinuclear region, interaction of PKD1 and 2 isoforms with SSH1L was not significantly different, emphasizing the specificity of the experimental approach (Supplemental Figure S5, D–I).

In summary, these data suggest that PKD1 may impair cancer cell motility and invasive properties by specific interaction with SSH1L at the cell periphery and phosphorylation of the Ser-978 substrate motif. To corroborate these findings, we also performed Transwell migration assays in Panc1 cells (Supplemental Figure S5J). In these experiments we used PKD1 and PKD2-GFP wild-type expression constructs to allow for a comparison of results with FRET studies. In line with our interaction studies for PKD isoforms, expression of PKD1-GFP, which was capable of efficiently interacting with SSH1L, significantly impaired motility of Panc1 cells by 59.7%. On the other hand, PKD2-GFP, which demonstrated strongly impaired

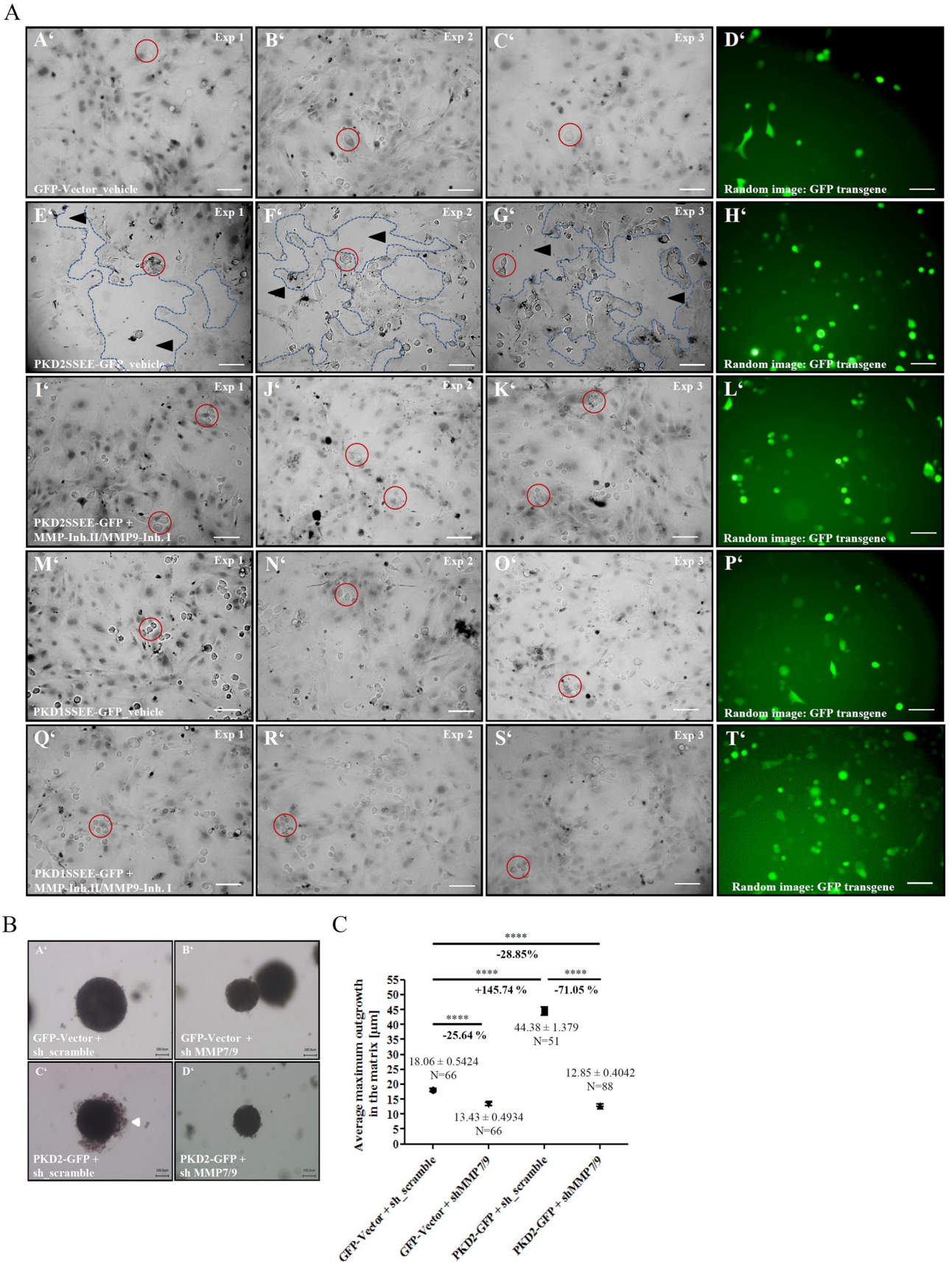

FIGURE 5: PKD1 and PKD2 control invasion of pancreatic cancer cells in an isoform-selective manner. PKD2 strongly enhances invasive properties of PDAC cells by secretion of MMPs. (A) Fibroblast overlay invasion assays were performed with Panc1 cells expressing GFP-Vector (A′–D′), constitutively active PKD2SSEE-GFP (E′– L′), or PKD1SSEE-GFP (M′– T′). Cells

interaction (by 77.3%), was able to inhibit migration by only ~18% (Supplemental Figure S5J). Thus migration assays after ectopic expression of wild-type PKD1 and 2 isoforms (Supplemental Figure S5J) further verify our findings, suggesting a strong isoform-selective, antimigratory/anti-invasive function of PKD1 as opposed to PKD2. To demonstrate regulation of SSH1L by PKD1 during invasion of cancer cells, we also assessed Transwell invasion assays performed with transiently transfected HeLa cells on Matrigel-coated filters (Supplemental Figure S5K). Analysis of three independent assays indicated that constitutively active PKD1SSEE impaired invasion through filters by ~50%. Expression of wild-type SSH1L, and even more pronounced for the SSH1LS978A mutant (phosphorylation ablated; Eiseler *et al.*, 2009b), significantly enhanced invasion compared with vector controls. Coexpression of constitutively active PKD1 with wild-type SSH1L again significantly impaired invasion to PKD1SSEE levels, whereas coexpressing PKD1 with the SSH1LS978A mutant fully reconstituted invasion to levels of the SSH1LS978A mutant without coexpression of PKD1 (Supplemental Figure S5K).

Thus, together with motility assays (Supplemental Figure S5J), these data indicate a functional inhibitory effect of PKD1 on tumor cell invasion, which is mediated by SSH1L phosphorylation at Ser-978 and most likely extends to various tumor cells and models, pointing to a general pattern for the regulation of cell motility via SSH1L selectively by the PKD1 isoform (Eiseler *et al.*, 2007, 2009a,b; Doppler *et al.*, 2013).

DISCUSSION

Early invasion and metastasis is a particular property of PDAC and constitutes a major challenge for novel therapeutic strategies. Here we demonstrate a novel, isoform-specific regulation of pancreatic cancer cell invasion by PKD1 and 2. PKD2 controls the invasive properties of pancreatic cancer cells at multiple levels. The kinase strongly enhances expression of MMP7/9 and regulates secretion (Pusapati *et al.*, 2010) at the TGN, as shown for the transport of MMP7/9 cargo (Supplemental Figure S3, A–E). We further demonstrate that MMP7 and 9 are responsible for the enhanced invasion of pancreatic cancer cells in 3D-ECM, fibroblast overlay invasion, and CAM models (Figure 5 and 6). MMP9 also increases PKD2-mediated tumor angiogenesis by controlling VEGF-A biorelease from cell surfaces and the ECM (Figure 6, E and F). Here MMP7 and 9 are likely to act in a common signaling cascade, given that MMP7 can process the MMP9 zymogen to its active state (Noel *et al.*, 1996; Wang *et al.*, 2005; Dozier *et al.*, 2006). By modulating expression and secretion of these two MMPs, PKD2 is even likely to exert control on the activity state of MMP9, broadly regulating angiogenesis signals at many levels (Azoitei *et al.*, 2010; Armacki *et al.*, 2013). Our data and published work from our lab further suggest that PKD2 is involved in the regulation of secretion from the TGN (Pusapati *et al.*, 2010). Of interest, enhanced secretion of MMP cargo seems to be PKD2 isoform specific (Supplemental Figure S3), although both PKD1 and 2 isoforms have been implicated in the regulation of vesicle fission from the TGN (Hausser *et al.*, 2005; Pusapati *et al.*, 2010). How this isoform specificity during secretion of MMPs is conveyed at the molecular level remains to be investigated and is of great interest to our future studies. Microarray expression data and our previous work suggest that PKD1 expression is comparably low in many PDACs (Seufferlein, 2002; Azoitei *et al.*, 2010; Porzner and Seufferlein, 2011). In breast cancer, there is a correlation between invasive tumor stages and low PKD1 expression levels (Eiseler *et al.*, 2009a). On the basis of our previous work and data presented in this study, we suggest that PKD1 increases tumor cell proliferation via Snail1 (Eiseler *et al.*, 2012) and could be necessary during early stages of tumor growth. At later stages of tumor progression, loss of PKD1 expression might even be an advantage for tumor cells to generate a high-migratory phenotype by exerting control over actin-regulatory proteins such as SSH1L (Supplemental Figure S5; Eiseler *et al.*, 2007, 2009b, 2010a; Doppler *et al.*, 2013). Our data further support a prominent anti-invasive, antimigratory role for PKD1 due to its strong isoform-selective interaction with SSH1L at the cell periphery and in motility-relevant peripheral membrane protrusions. Such an interaction is dramatically impaired for the PKD2 isoform (Supplemental Figure S5, D–I). Impaired interaction of PKD2 with SSH1L further resulted in a dramatically impaired ability to inhibit cell motility when compared with the PKD1 isoform (Supplemental Figure S5J). Loss of PKD1 in invasive tumors might therefore, at least in part, mediate antimigratory and thereby anti-invasive effects by an isoform-selective interaction with SSH1L. These data are not contradictory to published reports indicating regulation of SSH1L by phosphorylation via both isoforms (Peterburs *et al.*, 2009). We demonstrate, however, regulatory preferences for PKD1 in the cell periphery and parallel changes in cell motility, providing for the first time spatial information on the interaction with the actin-regulatory cofilin phosphatase and PKD1 substrate SSH1L. Via its regulation of cofilin activity SSH1L is significantly involved in the control of PKD1-dependent cancer cell motility, modulating the initial response of cells toward a chemotactic stimulus by generation of "barbed ends" and polymerization, driving membrane protrusion (Eiseler *et al.*, 2009b, 2010a). Emulating a situation of low PKD1 and high PKD2 expression in tumor cells, knockdown of PKD1 in PKD2-expressing pancreatic cancer cell lines revealed, in line with these findings, a highly invasive phenotype. Although PKD2 is upregulated in pancreatic cancer cells (Seufferlein, 2002; Azoitei *et al.*, 2010; Porzner and Seufferlein, 2011; Armacki *et al.*, 2013) due to impaired interaction with its substrate SSH1L in the cell periphery and our motility data (reduced by 77.3% for PKD2-GFP and by 83.4% for endogenous PKD2 vs. respective PKD1 controls), we suggest that anti-invasive/antimigratory properties of PKD2 in pancreatic

were additionally incubated either with vehicle or MMP-Inhibitor II/MMP9-Inhibitor I (1 µM/40 nM) when indicated. For invasion assays, 80,000 transfected Panc1 cells were seeded on dimethyl sulfoxide–inactivated (dead) mouse embryonal fibroblast monolayers in 12-well plates and incubated for 36 h in the presence or absence of inhibitors. Assays were documented at 10× magnification by acquiring five random images of monolayers using a Keyence microscope after labeling fibroblasts with trypan blue dye. Representative images for three independent assays and one random fluorescence image showing GFP-transgene expression (D′, H′, L′, P′, T′) are displayed for each experimental condition. Exemplary tumor cells growing on fibroblast monolayers are circled in red. Visibly penetrated fibroblast monolayers are marked with blue dotted linings. Scale bar, 100 µm. (B) 3D-BME invasion assays with stable cell lines expressing GFP-Vector as well as PKD2-GFP with nontargeting sh_scramble control or a MMP7/9 knockdown. Combined knockdown of MMP7/9 impairs invasiveness of PKD2-GFP–expressing Panc89 cells in 3D-ECM culture. Panc89 cell lines expressing the indicated constructs were seeded in ECM gel. Assays were documented at 8× magnification after 30 d. After 14 d, 500 µl of additional growth medium was added to 3D structures. Scale bar, 100 µm. (B) Average maximum outgrowth and SEM of three independent experiments. Statistical significance was calculated using two-tailed unpaired Student's *t* test.

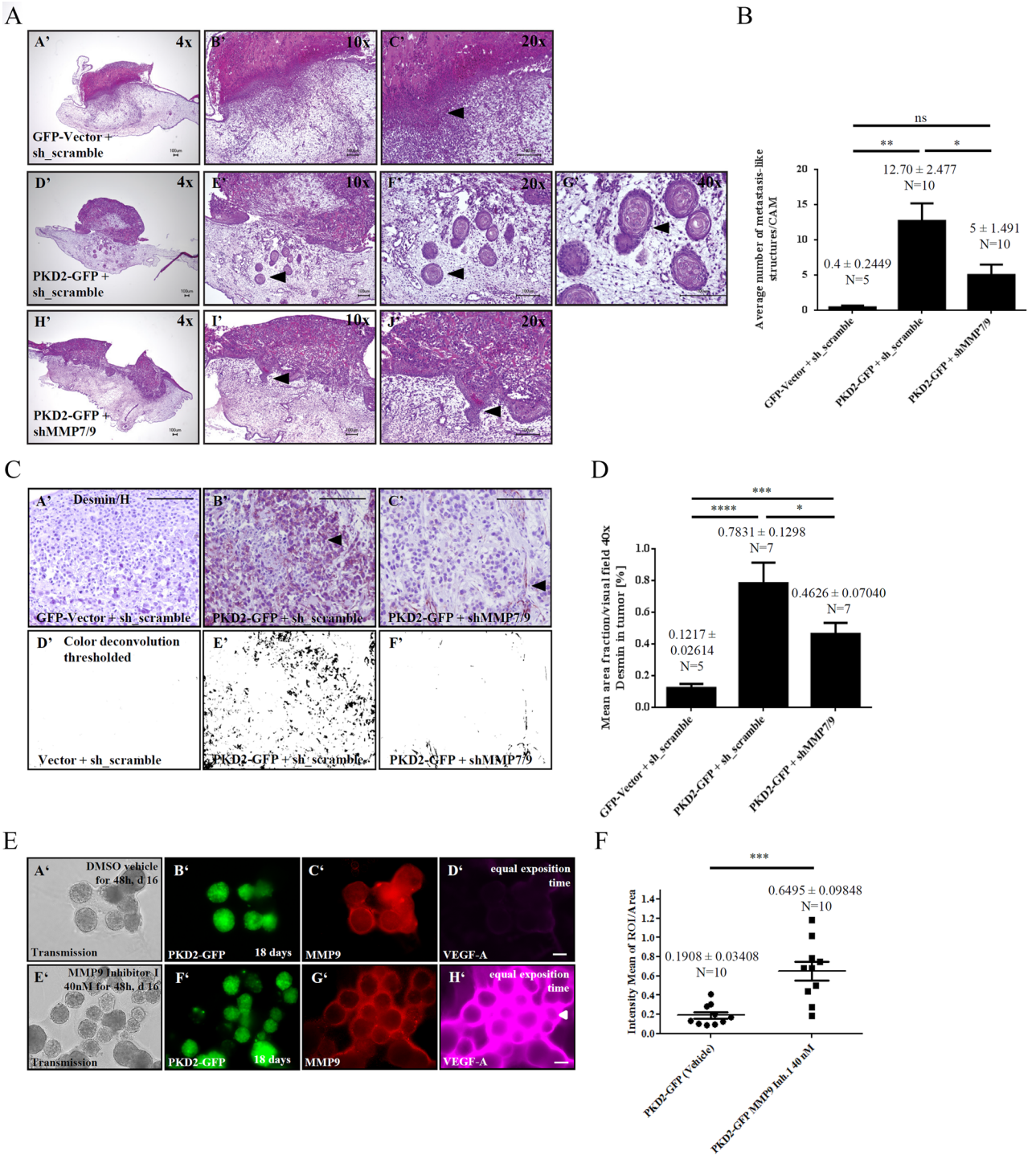

FIGURE 6: (A) Chorioallantois membrane assays with stable GFP-Vector + sh_scramble, PKD2-GFP + sh_scramble, and PKD2-GFP + shMMP7/9 Panc89 cell lines. Image panels display respective tumors at different magnifications. Scale bar, 100 µm. Arrowheads indicate tumor-CAM invasion fronts and metastasis-like structures (E′, F′) in CAM areas. (B) Knockdown of MMP7/9 significantly impairs formation of secondary structures. Statistical analysis of the average number of metastasis-like structures per CAM from at least three independent experiments was performed on stitched images (20×). Statistical significance was calculated using two-tailed unpaired Student's *t* test. (C) A′–C′, representative images of CAM sections at 40× magnification from within tumor areas stained for desmin and counterstained with hematoxylin (H); D′–F′, color deconvoluted, thresholded images of sections shown in A′–C′. Vascularization in tumors was quantified by calculating area fractions for desmin staining in images using ImageJ. (D) Quantification of desmin-stained tumor area fractions for five images per tumor as shown in C (D′–F′). Statistical significance was calculated using two-tailed unpaired Student's *t* test. (E) Inhibition of MMP9 significantly impairs VEGF-A release from a BME-matrix. PKD2-GFP–expressing Panc89 cell clusters were grown for 16 d. At day 16, 40 nM MMP9-Inhibitor I or vehicle control was added to assays for 48 h. After 18 d, clusters in the matrix were stained for MMP9 as well as VEGF-A and documented at 20× magnification using equal exposition settings for the VEGF-A channel with a Keyence BZ 9000 microscope. Scale, 100 µm. A′–D′,

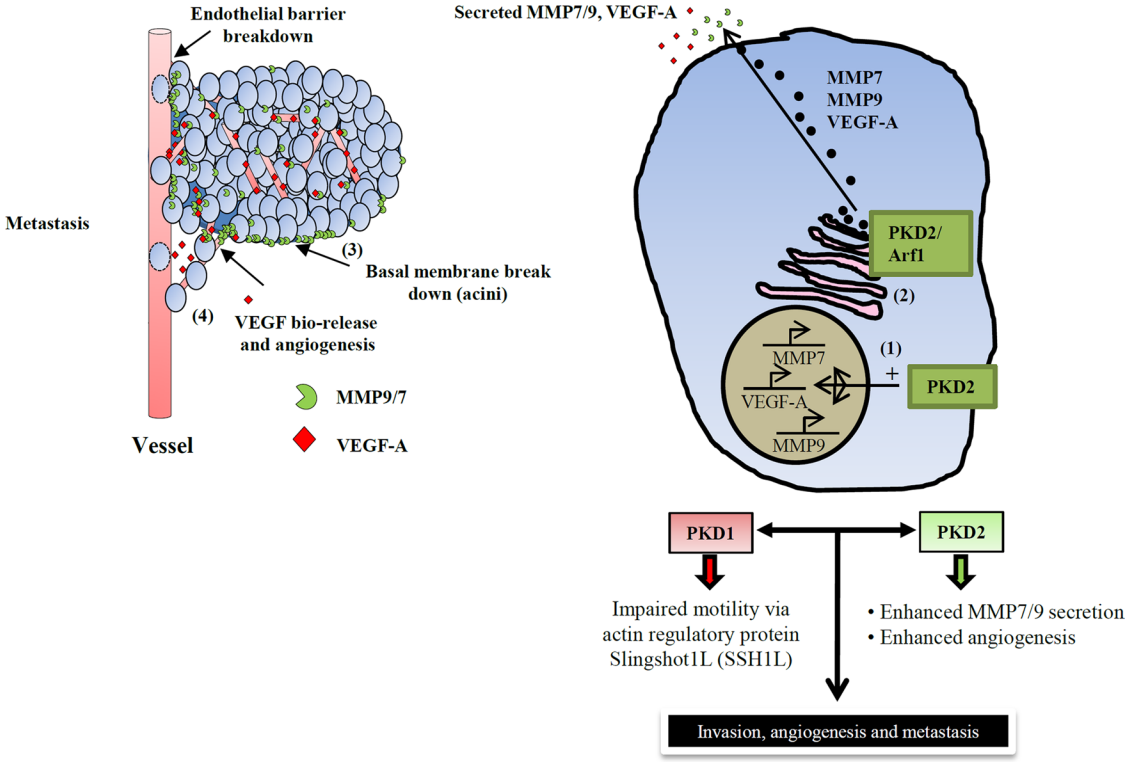

FIGURE 7: Overview of PKD2 functions in the control of pancreatic cancer cell and tumor invasion, as well as in angiogenesis. PKD2 regulates tumor invasiveness and angiogenesis at multiple levels: 1) PKD2 isoform–specific up-regulation of MMP7 and 9, as well as of VEGF-A. 2) PKD2 controls the constitutive secretion of MMP7 and 9 in an isoform-specific manner. 3) Secreted MMP7/9 enhance tumor cell invasiveness by degrading their respective ECM substrates. 4) Secreted MMP9 controls tumor angiogenesis mediated by PKD2, releasing VEGF-A from the ECM and tumor cluster surfaces. Cosecreted MMP7 may be able to further enhance the described MMP9-mediated functions by processing the zymogen (pro-MMP9) to the active protease. PKD1 mediates anti-invasive properties. In later stages of tumor progression before metastases, loss of PKD1 expression might be of advantage for tumor cells to generate a high-migratory phenotype by exerting control over actin-regulatory proteins such as SSH1L.

cancer cells are comparably weak, and thus the clearly proinvasive phenotype of PKD2 by massive induction of MMP7/9–driven invasion prevails (Figure 5 and Supplemental Figure S5).

Figure 7 shows a model of the opposing roles for PKD1 and 2 in PDAC. In conclusion, we demonstrate in an identical model system opposing PKD1 and 2 isoform–specific effects on pancreatic cancer cell invasion resembling a yin-yang situation for these PKD isoforms in PDAC. Kinase inhibitors are frequently used as targeted therapies in oncology. Our data highlight isoform specificity as an important feature of protein kinases in cancer and provide another line of argument for why general non–isoform-specific inhibitors of a kinase family sometimes do not exert the desired biological function in patients. PKD kinase inhibitors have already been proposed for the treatment of pancreatic cancer (Harikumar *et al.*, 2010).

In light of the data presented here, selective inhibitors targeting PKD2 rather than inhibiting all members of the PKD family should be developed.

MATERIALS AND METHODS

Cell culture, plasmids, antibodies, and dye reagents

Panc89 (PDAC), Panc1, MiaPaca, BxPC3, Capan1, HEK293T, and HeLa cells were maintained in RPMI media supplemented with 10% fetal calf serum (FCS) and penicillin/streptomycin. Panc1 cells were transfected using Turbofect (Fermentas, Schwerte, Germany), and small interfering RNAs (siRNAs) were transfected using Oligofectamine or Lipofectamine 2000 (Invitrogen, Life Technologies, Darmstadt, Germany). Experiments in HeLa cells were performed using HeLa Monster reagent (Mirus, Madison, WI). HEK293T cells were transfected using PEI (Polysciences, Warrington, PA). Panc1, HEK293T, HeLa cells, and PDAC cell lines were acquired from the American Type Culture Collection or DSMZ–German Collection of Microorganisms and Cell Cultures. Stable Panc89 cells used in this study were described previously (Eiseler *et al.*, 2007, 2010b). Stable knockdowns using shRNAs were performed by lentiviral transduction. Production of lentiviruses has been described previously (Eiseler *et al.*, 2012). GFP-tagged and pcDNA3 expression constructs for PKD1, PKD1SSEE, PKD2, and PKD2SSEE have been published (Hausser *et al.*, 2002; Eiseler *et al.*, 2007). MMP7-YFP and YFP-MMP9 were purchased from Source Bioscience. MMP9-GFP (mouse) was a kind gift of M. Khrestchatisky (Centre National de la Recherche Scientifique, Marseille, France). shRNAs against lacz, PKD1, PKD2, and PKD3 were described previously (Eiseler *et al.*, 2010a, 2012) and purchased from MWG Biotech, Ebersberg, Germany. Control shRNA and shRNA constructs against PKD1 and

vehicle controls; E′–H′, clusters incubated with MMP9-Inhibitor 1. Images shown were omitted from quantitative analysis due to saturated pixel values in H′. (F) Quantitative analysis of VEGF-A intensity per area quantified from ROIs including the surrounding matrix. Ten black-level background images with nonsaturated staining per condition were used for quantitative analysis. Statistical significance was calculated using two-tailed unpaired Student's *t* test.

PKD2 were purchased from Sigma-Aldrich, St. Louis, MO (control shRNA [Mission shRNA, Sigma shc002], PKD1 shRNA [PKD1 shRNA NM_002742.x-2978s1c1], PKD2 shRNA [sh PKD2 #1, NM_016457.x-1720s1c1; and sh PKD2 #2, NM_016457.x-294s1c1]). pGIPz shRNA constructs against MMP7 (V2LHS_151821 NM_002423) and MMP9 (V2LHS_248918 NM_004995) were acquired from Open Biosystems, Thermo Scientific, Schwerte, Germany. Anti-actin and anti-tubulin antibodies were purchased from Sigma-Aldrich. Anti-GFP antibody was acquired from Roche, Mannheim, Germany. Anti-PKD1 (C20) was obtained from Santa Cruz Biotechnology, Dallas, TX. Anti-PKD2 antibody was from Calbiochem, Merk Group, Darmstadt, Germany. Anti-MMP9 was purchased from Cell Signaling, Boston, MA. MMP7 antibody was purchased from Abnova, Taipei City, Taiwan. Anti-VEGF-A antibody was acquired from Abcam, Cambridge, UK. The human MMP9 enzyme-linked immunosorbent assay kit was purchased from Invitrogen. Anti-desmin and pan-cytokeratin antibodies were from DAKO, Glostrup, Denmark. Immunofluorescence and immunohistochemistry secondary reagents were purchased from Invitrogen and DAKO, respectively. Quantitative PCR primers were obtained from Qiagen, Hilden, Germany.

Total cell lysates and Western blotting

In brief, total cell lysates were prepared by solubilizing cells in lysis buffer (50 mM Tris, pH 7.4, 150 mM NaCl, 5 mM $MgCl_2$, 1% Triton X-100) plus Complete protease and PhosStop inhibitors (Roche). Lysates were subjected to SDS–PAGE, blotted, and probed with specific antibodies. Proteins were visualized by horseradish peroxidase–coupled secondary antibodies using enhanced chemiluminescence (Thermo Fisher). Quantitative analysis of Western blots was done by measuring integrated band density using ImageJ (National Institutes of Health, Bethesda, MD).

Quantitative real-time PCR

Quantitative real-time PCR (qPCR) was performed in a BioRad iQ5 cycler with SYBR Green from 400 ng of total RNA after cDNA synthesis. qPCR analysis was performed in three replicas from at least three independent experiments. Results were calculated according to the $\Delta\Delta Ct$ method normalized to glyceraldehyde-3-phosphate dehydrogenase and vector control cells.

Transwell migration, invasion, and 3D-ECM assays

Transwell migration assays using transiently transfected Panc1 cells were performed as follows. Transfected Panc1 cells (300,000/filter) were seeded on 12-well Transwell inserts with 8-µm pore diameter (BD-Bioscience, Heidelberg, Germany). Migration was induced by an FCS gradient (0.1% bovine serum albumin [BSA] to 10% FCS) for 16 h. Assays were stopped by fixation with 4% formaldehyde. Nonmigratory cells on top of filters were removed with a cotton swab, and the remaining cells on filter membranes were stained with 4′,6-diamidino-2-phenylindole (DAPI). Migration was quantified by documenting DAPI-stained nuclei on filters with a Keyence fluorescence microscope at 10× magnification. For statistical analysis nine random images per filter, two replica filters per condition, and three independent experiments were analyzed by counting the number of stained nuclei (ImageJ). Results are presented as average number of cells/visual field for all replica assays.

Transwell invasion assays were performed with Matrigel-coated filters in 12-well plates (4 µg/filter), two replica filters per condition, and three independent experiments. Invasion of cells was induced by a gradient of 0.1% BSA to 10% FCS with 300,000 HeLa cells for 16 h. For documentation, filters were fixed with 4% formaldehyde, cells on the upper side of filters were removed by a cotton swab, and invading cells were stained with DAPI. Assays were documented by acquiring 20× images of DAPI-stained nuclei on filters with nine images per filter using a Keyence BZ 9000 fluorescence microscope (Neu-Isenburg, Germany). Nuclei were subsequently counted automatically utilizing an ImageJ macro applying size exclusion filters to exclude cells stuck in filter pores. Results are shown as average number of cells/visual field that passed through Matrigel-coated filter membranes.

The 3D-BME culture was performed by seeding 10,000 singular cells/24 wells of stable Panc89 cell lines (Eiseler *et al.*, 2007, 2010b) in BME (growth factor reduced, phenol red free; Cultrex; R&D Systems, Gaithersburg, MD). Tumor cell clusters were treated as indicated and documented after the stated time points using a Keyence BZ 9000 microscope. Invasive stellate outgrowth in the surrounding matrix was quantified at five positions around clusters, with no more than three measurements within the same outgrowth area using spatial calibration of images (ImageJ).

Fibroblast overlay invasion assays

Fibroblast overlay invasion assays with invasive Panc1 cells were performed as follows. Low-passage mouse embryonal fibroblasts were seeded in 12-well plates and grown to confluent monolayers. Fibroblasts were inactivated by incubation with dimethyl sulfoxide for 20 min at room temperature. Panc1 cells were transfected in six-well plates using Turbofect (Fermentas), applying a standard protocol. After intensive washing steps, 80,000 transfected Panc1 cells were seeded on top of the fibroblast monolayers. After initial adhesion for 4 h, vehicle and inhibitors w ere added as indicated. After 36 h, random fluorescence images of GFP-transfected Panc1 cells were acquired for all assays, and invasion of tumors cells in the fibroblast monolayers was subsequently documented by visualizing the integrity of fibroblast monolayers after staining with trypan blue solution for 10 min after washing once with phosphate-buffered saline (PBS). Three independent assays were documented with five random bright-field images at 10× magnification using a Keyence BZ 9000 microscope.

Immunofluorescence, acceptor-photobleach FRET, and confocal microscopy

HeLa and Panc1 cells were seeded on glass coverslips, transfected as indicated, and processed as described in Eiseler *et al.* (2012). Samples were analyzed by a confocal laser scanning microscope, LSM710 (Zeiss, Jena, Germany) or TCS SP5 (Leica, Wetzlar, Germany), equipped with respective 63× Plan Apo oil or 40× water immersion objective. Images were acquired in sequential scan mode. Acceptor-photobleach FRET measurements were carried out by acquiring prebleach and postbleach images of donor and acceptor. The acceptor was bleached using an intensive 561-nm laser line. Quantitative analysis was performed by placing sub-ROIs within the beach ROI as stated in Supplemental Figure S5, D–I, calculating single percentage FRET values, as well as mean FRET efficiency and SEM of nonthresholded raw data. Statistical significance was calculated using two-tailed unpaired Student's *t* test.

Secretion assays with MMP cargo

HEK239T cells were seeded at a density of 400.000 cells/well in six-well dishes. On the following day, cells were transfected with the indicated siRNA constructs. The next day cells were transfected with MMP7-YFP and YFP-MMP9 cargo. Five hours after the second transfection, cells were washed two times with PBS, and normal growth medium was replaced with serum-free medium. After 24 h of secretion, supernatants were harvested, resolved by SDS gels, and analyzed by Western blotting and densiometry.

Modified FRAP approach to measure cargo vesicle release from the TGN

For indirect measurement of MMP9-GFP cargo vesicle release from the TGN we used a modified FRAP approach. FRAP experiments with MMP9-GFP cargo were acquired using a Leica TCS SP5 confocal microscope equipped with a 100× oil immersion objective at 37°C and 5% CO_2. HeLa cells were seeded on glass-bottom dishes (MatTek, Ashland, MA) and transfected with constitutively active, nontagged pcDNA3-PKD1SSEE and PKD2SSEE or empty vector constructs together with MMP9-GFP at a ratio of 3:1. FRAP time–bleach series of TGN-accumulated MMP9-GFP were recorded in phenol red–free media using 90% open pinholes to compensate for dynamic movements of Golgi structures.

Gelatin zymography for MMP9 and MMP7

Gelatin zymography and heparin-enhanced zymography were performed as described (Kleiner and Stetler-Stevenson, 1994; Snoek-van Beurden and Von den Hoff, 2005). In brief, FCS-free supernatants from cells containing secreted MMPs were concentrated using Vivaspin2 filters (MWCO 10,000; Satorius Stedim, Goettingen, Germany) and incubated with 2× Tris-glycine SDS sample buffer for 10 min at room temperature. Supernatants for MMP9 were resolved on 10% zymography gels containing 1 mg/ml gelatin, and for detection of MMP7 activity, samples were in addition resolved with heparin (3 µg/lane). After renaturation (2.5% Triton X-100) for 30 min, gels were washed once in developing buffer (50 mM Tris, pH 8, 0.2 M NaCl, 5 mM $CaCl_2$, and 0.02% Brij 35) for 30 min and further incubated overnight for enhanced sensitivity at 37°C. The MMP reaction was stopped by incubation of gels in Coomassie solution. After destaining, active MMPs were distinguishable by white bands at the respective molecular weight in supernatant lanes.

Immunohistochemistry in-gel staining and quantitative intensity analysis of tumor clusters from 3D BME assays

Tumor cluster in the BME matrix was fixed with 4% formaldehyde for 20 min at room temperature, washed, and pipetted together with matrix on a microscopy slide. Clusters were air dried for 2 h and permeabilized with 0.1% Triton X-100. Samples were treated as indicated in the description of immunofluorescence staining and analyzed by a Keyence 9000 fluorescence microscope at 20× magnification. Quantitative intensity analysis was performed as in Figure 6F.

Chorioallantois membrane assays

Shells of fertilized chicken eggs were opened on day 4, and 5-mm silicon rings were applied onto the CAM (Azoitei *et al.*, 2010). Stable Panc89 cell lines expressing the indicated constructs (2×10^6) were mixed with Matrigel in ratio of 1:1 (BD Matrigel, 10 µg/µl; Becton Dickinson) and transplanted onto the CAM. Tumors were photographed and harvested after 4 d. Formalin-fixed tumors were embedded in paraffin using standard histological procedures. The 5-µm sections were processed and stained as indicated in the figures. Images were acquired using a Keyence 9000 microscope.

Statistical analysis

Statistical analysis was performed using Prism software, version 5.00, for Windows (GraphPad, San Diego, CA). Statistical significance: $*p = 0.05–0.01$, $**p = 0.01–0.001$, $***p < 0.001$, $****p < 0.0001$.

ACKNOWLEDGMENTS

This work was funded by Deutsche Krebshilfe Grant 109222 and Deutsche Forschungsgemeinschaft grant EI792/3-1 to T.E., as well as by Deutsche Krebshilfe Grant 109373 to T.S. We thank Klaus Pfizenmaier for critical reading of the manuscript and helpful comments.

REFERENCES

Armacki M, Joodi G, Nimmagadda SC, de Kimpe L, Pusapati GV, Vandoninck S, Van Lint J, Illing A, Seufferlein T (2013). A novel splice variant of calcium and integrin-binding protein 1 mediates protein kinase D2-stimulated tumour growth by regulating angiogenesis. Oncogene, doi:10.1038/onc.2013.43.

Azoitei N *et al.* (2010). Protein kinase D2 is a crucial regulator of tumour cell-endothelial cell communication in gastrointestinal tumours. Gut 59, 1316–1330.

Beil M, Leser J, Lutz MP, Gukovskaya A, Seufferlein T, Lynch G, Pandol SJ, Adler G (2002). Caspase 8-mediated cleavage of plectin precedes F-actin breakdown in acinar cells during pancreatitis. Am J Physiol Gastrointest Liver Physiol 282, G450–G460.

Bergers G, Benjamin LE (2003). Tumorigenesis and the angiogenic switch. Nat Rev Cancer 3, 401–410.

Bergers G *et al.* (2000). Matrix metalloproteinase-9 triggers the angiogenic switch during carcinogenesis. Nat Cell Biol 2, 737–744.

Biswas MH, Du C, Zhang C, Straubhaar J, Languino LR, Balaji KC (2010). Protein kinase D1 inhibits cell proliferation through matrix metalloproteinase-2 and matrix metalloproteinase-9 secretion in prostate cancer. Cancer Res 70, 2095–2104.

Crawford HC, Scoggins CR, Washington MK, Matrisian LM, Leach SD (2002). Matrix metalloproteinase-7 is expressed by pancreatic cancer precursors and regulates acinar-to-ductal metaplasia in exocrine pancreas. J Clin Invest 109, 1437–1444.

del Castillo CF, Warshaw L (1993). Peritoneal metastases in pancreatic carcinoma. Hepatogastroenterology 40, 430–432.

Doppler H, Bastea LI, Eiseler T, Storz P (2013). Neuregulin mediates F-actin-driven cell migration through inhibition of protein kinase D1 via Rac1 protein. J Biol Chem 288, 455–465.

Dozier S, Escobar GP, Lindsey ML (2006). Matrix metalloproteinase (MMP)-7 activates MMP-8 but not MMP-13. Med Chem 2, 523–526.

Egeblad M, Werb Z (2002). New functions for the matrix metalloproteinases in cancer progression. Nat Rev Cancer 2, 161–174.

Eiseler T, Doppler H, Yan IK, Goodison S, Storz P (2009a). Protein kinase D1 regulates matrix metalloproteinase expression and inhibits breast cancer cell invasion. Breast Cancer Res 11, R13.

Eiseler T, Doppler H, Yan IK, Kitatani K, Mizuno K, Storz P (2009b). Protein kinase D1 regulates cofilin-mediated F-actin reorganization and cell motility through slingshot. Nat Cell Biol 11, 545–556.

Eiseler T, Hausser A, De Kimpe L, Van Lint J, Pfizenmaier K (2010a). Protein kinase D controls actin polymerization and cell motility through phosphorylation of cortactin. J Biol Chem 285, 18672–18683.

Eiseler T, Hausser A, De Kimpe L, Van Lint J, Pfizenmaier K (2010b). Protein kinase D controls actin polymerization and cell motility through phosphorylation of cortactin. J Bio Chem 285, 2418672–18683.

Eiseler T, Kohler C, Nimmagadda SC, Jamali A, Funk N, Joodi G, Storz P, Seufferlein T (2012). Protein kinase D1 mediates anchorage-dependent and -independent growth of tumor cells via the zinc finger transcription factor Snail1. J Biol Chem 287, 32367–32380.

Eiseler T, Schmid MA, Topbas F, Pfizenmaier K, Hausser A (2007). PKD is recruited to sites of actin remodelling at the leading edge and negatively regulates cell migration. FEBS Lett 581, 4279–4287.

Guha S, Tanasanvimon S, Sinnett-Smith J, Rozengurt E (2010). Role of protein kinase D signaling in pancreatic cancer. Biochem Pharmacol 80, 1946–1954.

Harikumar KB *et al.* (2010). A novel small-molecule inhibitor of protein kinase D blocks pancreatic cancer growth in vitro and in vivo. Mol Cancer Ther 9, 1136–1146.

Hausser A, Link G, Bamberg L, Burzlaff A, Lutz S, Pfizenmaier K, Johannes FJ (2002). Structural requirements for localization and activation of protein kinase C mu (PKC mu) at the Golgi compartment. J Cell Biol 156, 65–74.

Hausser A, Storz P, Martens S, Link G, Toker A, Pfizenmaier K (2005). Protein kinase D regulates vesicular transport by phosphorylating and activating phosphatidylinositol-4 kinase IIIbeta at the Golgi complex. Nat Cell Biol 7, 880–886.

Kessenbrock K, Plaks V, Werb Z (2010). Matrix metalloproteinases: regulators of the tumor microenvironment. Cell 141, 52–67.

Kleiner DE, Stetler-Stevenson WG (1994). Quantitative zymography: detection of picogram quantities of gelatinases. Analyt Biochem 218, 325–329.
Korc M (2003). Pathways for aberrant angiogenesis in pancreatic cancer. Mol Cancer 2, 8.
LaValle CR, Zhang L, Xu S, Eiseman JL, Wang QJ (2012). Inducible silencing of protein kinase D3 inhibits secretion of tumor-promoting factors in prostate cancer. Mol Cancer Ther 11, 1389–1399.
Masson V *et al*. (2005). Contribution of host MMP-2 and MMP-9 to promote tumor vascularization and invasion of malignant keratinocytes. FASEB J 19, 234–236.
Maupin KA *et al*. (2010). Glycogene expression alterations associated with pancreatic cancer epithelial-mesenchymal transition in complementary model systems. PloS One 5, e13002.
Merikallio H, Turpeenniemi-Hujanen T, Paakko P, Makitaro R, Riitta K, Salo S, Salo T, Harju T, Soini Y (2012). Snail promotes an invasive phenotype in lung carcinoma. Respir Res 13, 104.
Noel AC, Lefebvre O, Maquoi E, VanHoorde L, Chenard MP, Mareel M, Foidart JM, Basset P, Rio MC (1996). Stromelysin-3 expression promotes tumor take in nude mice. J Clin Invest 97, 1924–1930.
Page-McCaw A, Ewald AJ, Werb Z (2007). Matrix metalloproteinases and the regulation of tissue remodelling. Nat Rev Mol Cell Biol 8, 221–233.
Pei H, Li L, Fridley BL, Jenkins GD, Kalari KR, Lingle W, Petersen G, Lou Z, Wang L (2009). FKBP51 affects cancer cell response to chemotherapy by negatively regulating Akt. Cancer Cell 16, 259–266.
Peterburs P, Heering J, Link G, Pfizenmaier K, Olayioye MA, Hausser A (2009). Protein kinase D regulates cell migration by direct phosphorylation of the cofilin phosphatase slingshot 1 like. Cancer Res 69, 5634–5638.
Porzner M, Seufferlein T (2011). Novel approaches to target pancreatic cancer. Curr Cancer Drug Targets 11, 698–713.
Pusapati GV, Krndija D, Armacki M, von Wichert G, von Blume J, Malhotra V, Adler G, Seufferlein T (2010). Role of the second cysteine-rich domain and Pro275 in protein kinase D2 interaction with ADP-ribosylation factor 1, *trans*-Golgi network recruitment, and protein transport. Mol Biol Cell 21, 1011–1022.
Rasmussen HS, McCann PP (1997). Matrix metalloproteinase inhibition as a novel anticancer strategy: a review with special focus on batimastat and marimastat. Pharmacol Ther 75, 69–75.
Rykx A, De Kimpe L, Mikhalap S, Vantus T, Seufferlein T, Vandenheede JR, Van Lint J (2003). Protein kinase D: a family affair. FEBS Lett 546, 81–86.
Seufferlein T (2002). Novel protein kinases in pancreatic cell growth and cancer. Int J Gastrointest Cancer 31, 15–21.
Snoek-van Beurden PA, Von den Hoff JW (2005). Zymographic techniques for the analysis of matrix metalloproteinases and their inhibitors. BioTechniques 38, 73–83.
Tsuzuki Y, Mouta Carreira C, Bockhorn M, Xu L, Jain RK, Fukumura D (2001). Pancreas microenvironment promotes VEGF expression and tumor growth: novel window models for pancreatic tumor angiogenesis and microcirculation. Lab Invest 81, 1439–1451.
Wang FQ, So J, Reierstad S, Fishman DA (2005). Matrilysin (MMP-7) promotes invasion of ovarian cancer cells by activation of progelatinase. Int J Cancer 114, 19–31.
Werb Z (1997). ECM and cell surface proteolysis: regulating cellular ecology. Cell 91, 439–442.
Yeaman C *et al*. (2004). Protein kinase D regulates basolateral membrane protein exit from trans-Golgi network. Nat Cell Biol 6, 106–112.
Yoo J, Rodriguez Perez CE, Nie W, Sinnett-Smith J, Rozengurt E (2011). Protein kinase D1 mediates synergistic MMP-3 expression induced by TNF-alpha and bradykinin in human colonic myofibroblasts. Biochem Biophys Res Commun 413, 30–35.